Heliyon 10 (2024) e35700

Contents lists available at ScienceDirect

Heliyon

journal homepage: www.cell.com/heliyon

Research article

Comprehensive analysis of cuproptosis-related ceRNA network and immune infiltration in diabetic kidney disease

Fang Lan [a], Jie Zhao [a], Dan Liang [b], Chao Mo [a,b,1,*], Wei Shi [a,**,1]

[a] Department of Nephrology, the First Affiliated Hospital of Guangxi University of Chinese Medicine, Nanning, Guangxi, 530023, PR China
[b] Graduate School, Guangxi University of Chinese Medicine, Nanning, Guangxi, 530200, PR China

ARTICLE INFO

Keywords:
Diabetic kidney disease
Cuproptosis
ceRNA network
Immune infiltration

ABSTRACT

Background: Diabetic kidney disease (DKD) is the primary contributor to renal failure and poses a severe threat to human health. Accumulating studies demonstrated that competing endogenous RNA (ceRNA) network is involved in cuproptosis and DKD progression. However, the role of cuproptosis-associated ceRNA network and immune infiltration in DKD remains largely unclear. This study aimed to investigate the cuproptosis-related ceRNA regulation network and immune infiltration in DKD.

Methods: The rat model of DKD was induced by combining the nephrectomy of the left kidney, high-fat diet, and streptozotocin. Differentially expressed genes (DEGs), miRNAs (DEMs), and lncRNAs (DELs) between normal and DKD rats were obtained. DEGs were intersected with cuproptosis-related genes (CRGs) to obtain DE-CRGs. LncRNAs and miRNAs were predicted based on the DE-CRGs, and they were intersected with DEMs and DELs, respectively. Subsequently, a cuproptosis-associated lncRNA-miRNA-mRNA network was established in DKD. In addition, the relative proportion of 22 infiltrating immune cell types in each sample was calculated, and the relationship between hub DE-CRGs and immune cells was explored.

Results: In total, there were 429 DEGs, 22 DEMs, and 48 DELs between CON and MOD groups. Then, 73 DE-CRGs were obtained, which were significantly enriched in 22 pathways, such as MAPK signaling pathway, IL-17 signaling pathway, and TNF signaling pathway. In addition, a core cuproptosis-related ceRNA network that included one lncRNA (USR0000B2476D), one miRNA (miR-34a-3p), and eight mRNAs (Mmp9, Pik3c3, Prom1, Snta1, Slc51b, Ntrk3, Snca, Egf) was established. In addition, 18 hub DE-CRGs were obtained. CIBERSORT algorithms showed that resting dendritic cells and resting NK cells were more infiltrated whereas regulatory T cells were less infiltrated in DKD rats than in normal rats. Spearman's correlation analysis revealed that hub DE-CRGs showed significant positive or negative correlations with naive B cells, regulatory T cells, resting NK cells, M0 macrophages, resting dendritic cells, and resting mast cells.

Conclusion: A ceRNA network was comprehensively constructed, and 18 hub DE-CRGs were obtained, which will provide novel insights into the pathologic mechanism elucidation and targeted therapy development of DKD.

* Corresponding author. Department of Nephrology, the First Affiliated Hospital of Guangxi University of Chinese Medicine, No.89-9 Dongge Road, Qingxiu District, Nanning, Guangxi, 530023, PR China.
** Corresponding author.
E-mail addresses: lanfang77@163.com (F. Lan), zhaojie9520@163.com (J. Zhao), 3112508204@qq.com (D. Liang), mochao19890321@163.com (C. Mo), shiw1960@163.com (W. Shi).
[1] Chao Mo and Wei Shi are the co-corresponding authors

https://doi.org/10.1016/j.heliyon.2024.e35700
Received 31 May 2024; Received in revised form 31 July 2024; Accepted 1 August 2024
Available online 8 August 2024

1. Introduction

Diabetes mellitus (DM) is a serious threat to humanity's health today. According to data reported by the International Diabetes Federation, there will be an estimated 780 million people living with DM in 2045 [1]. Among them, approximately 20 %–40 % of individuals with DM develop diabetic kidney disease (DKD) [2]. DKD is a common, devastating, and expensive microvascular complication of DM and is currently the leading cause of end-stage renal disease worldwide [3]. Worse yet, patients with DKD are at higher cardiovascular events, hospitalizations, and mortality risks than those with only DM [4,5]. In contrast to a decline in other diabetic complications, a similar phenomenon has not been observed in DKD [6]. DKD can be caused by multiple factors, such as hyperglycemia, hypertension, inflammation, and oxidative stress; nevertheless, there is a lack of perfect mechanisms to explain DKD [7]. Although current therapies for DKD, including lifestyle changes, controlling hyperglycemia and hypertension, as well as improving hyperlipidemia have been modestly successful [3], a large residual risk for the onset or/and progression of DKD remains [8]. These data indicate that investigating comprehensive mechanisms of DKD is meaningful for identifying novel targets and therapeutic methods.

Copper is an essential micronutrient of biological processes to maintain systemic copper homeostasis; yet, excessive copper causes cell metabolic dysfunction [9]. Cuproptosis, namely, excessive copper contributes to abnormal lipoacylated protein aggregation, interferes with iron-sulfur tuftin associated with mitochondrial respiration, causes proteotoxic stress response, and ultimately leads to cell death [10]. In contrast to previously described various cell death, such as apoptosis, pyroptosis, necroptosis, and ferroptosis, cuproptosis is a novel form of copper-dependent, non-apoptotic, non-ferrous, and non-necrotic programmed cell death [11]. Accumulating studies have shown that copper homeostasis and cuproptosis play important regulatory roles in the progression of multiple diseases, such as tumors [12], cardiovascular diseases [13], and cerebral diseases [14]. It has been reported that cuproptosis-related RNAs, such as long non-coding RNAs (lncRNAs), microRNAs (miRNAs), and mRNAs, are involved in the disease prognosis and associated with immune infiltration [15,16]. In addition, cuproptosis-related non-coding RNAs and protein-coding mRNAs are linked via competing endogenous RNA (ceRNA) networks to promote disease progression. For instance, the LINC00511/miR-29c-3p/SLC31A1 axis promoted breast cancer progress via regulating copper transport [17]. However, studies on the potential roles of the cuproptosis-related ceRNA network and the relationship between cuproptosis and immune infiltration in DKD have not been reported yet. Thus, this study is the first to comprehensively analyze the potential mechanisms of cuproptosis-associated ceRNA network and immune infiltration in DKD.

In this study, we carried out RNA high-throughput sequencing, including lncRNA, miRNA, and mRNA, of kidney tissues in normal and DKD model rats. Differentially expressed (DE) lncRNAs, miRNAs, and mRNAs were obtained, and DE mRNAs were intersected with cuproptosis-related genes (CRGs) to acquire DE-CRGs. In addition, cuproptosis-related lncRNA and miRNA were predicted based on the DE-CRGs. A regulatory ceRNA network with DE-CR lncRNAs, miRNAs, and mRNAs was established to reveal the potential influence on DKD. Subsequently, the relative proportion of 22 infiltrating immune cell types in each sample was calculated, and the relationship between hub DE-CRGs and immune cells was explored. Our study may reveal the most potential cuproptosis-related ceRNA network in the DKD progress and therapeutic targets for DKD by regulating copper transport, which may provide a new perspective on DKD and guidelines for further experimental research. The flowchart of this study is shown in Fig. 1.

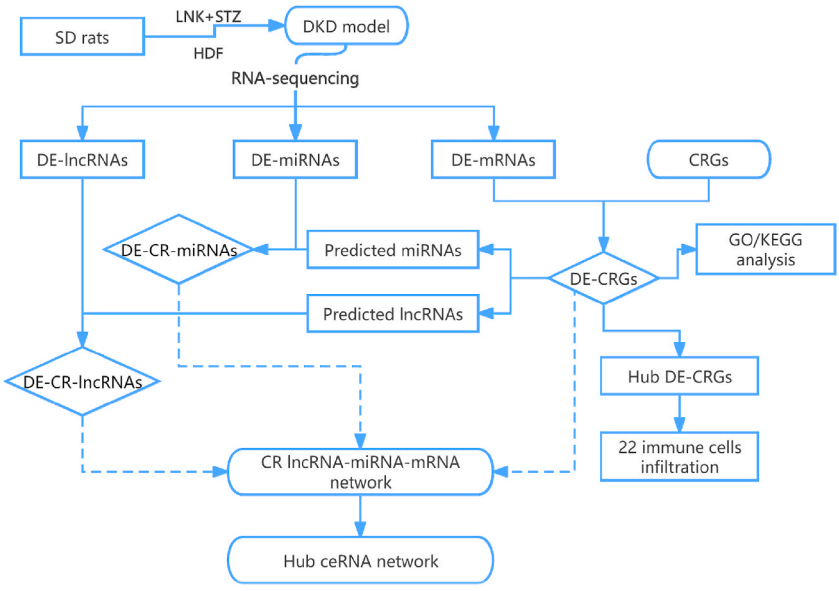

Fig. 1. Flow chart of the present study. CRGs, cuproptosis-related genes; DKD, diabetic kidney disease; DE, differentially expressed; HDF, high-fat diet; LKN, nephrectomy of the left kidney; SD, Sprague Dawley; STZ, streptozocin.

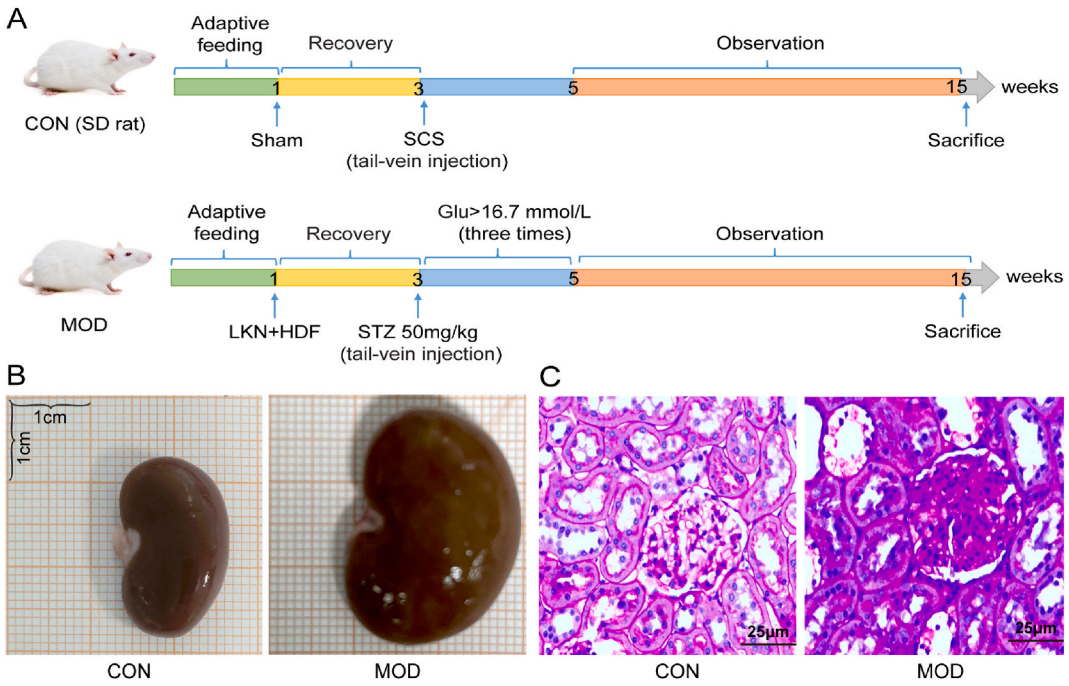

Fig. 2. DKD model and histological analysis. (A) The procedure of DKD model. (B) Kidney size of CON and MOD groups. (C) PAS staining of kidney tissue in CON and MOD groups. MOD, model group; SD, Sprague Dawley; SCS, sodium-citrate solution; LKN, nephrectomy of the left kidney; HDF, high-fat diet; STZ, streptozocin; CLU, blood glucose.

2. Materials and methods

2.1. Animal model preparation

Six male 5-week-old Sprague Dawley (SD) rats were obtained from Hunan Slack Jingda Experimental Animal Co., LTD (Changsha, China; animal license No. SYXK(Gui)2019-0001). Rats were kept in specific-pathogen-free conditions with a temperature of 22 ± 2 °C, a 12-h light/dark cycle, along with humidity of 60 ± 5 %, and had access to drink and normal rat chow ad libitum.

A DKD rat model was established by combining nephrectomy of the left kidney, high-fat diet (HDF), and streptozotocin treatment in our experiment, as previously described [18–21]. After one week of adaptive feeding, rats were randomly divided into two groups, that is, the normal control group (CON, n = 3) and the model group (MOD, n = 3). Rats in the CON group underwent sham-operated surgery, while rats in the MOD group were subjected to nephrectomy of the left kidney under isoflurane (Ringpu, Tianjin, China) anesthesia (3 %–4 % induction, 1.5 %–2.5 % maintenance, as well as 100 % oxygen). Rats received analgesia after the surgery via subcutaneous injection of 0.2 mg/kg meloxicam injection (Kangdien, Qingdao, China) for five consecutive days. After one day of surgery, rats were fed a normal chow diet (CON, n = 3) or HDF with 17 % kcal protein, 32 % kcal fat, and 51 % kcal carbohydrate (MOD, n = 3). After two weeks of recovery, 50 mg/kg STZ (Sigma-Aldrich, St Louis, USA) dissolved in 0.1M sodium-citrate solution (pH 4.5) was injected into HFD-fed rats through tail-vein injection for one day. Meanwhile, rats in the CON group received 100 μL of 0.1M sodium-citrate solution (pH 4.5). After STZ treatment 72 h, blood glucose levels were measured from the tail vein by using an Accu-Chek glucometer (Roche, Mannheim, Germany) for three consecutive days, and rats with three or more random blood glucose >16.7 mmol/L were considered successful models. On the fifteenth week, all rats were anesthetized with isoflurane, and kidney tissues were collected. Subsequently, each kidney was divided into two parts, of which one part was fixed in 4 % paraformaldehyde for 24 h and the other part was snap-frozen in liquid nitrogen for the following analysis. The procedure of animal model preparation is exhibited in Fig. 2A.

2.2. Histopathological analysis of kidney

The 4 % paraformaldehyde-fixed kidney tissues were embedded in paraffin and were sectioned into 5 μm slices. The kidney sections were stained with Periodic acid-Schiff (PAS), according to a standard protocol. Histopathological features of kidney tissues were observed using a microscope (Olympus, Tokyo, Japan).

2.3. RNA extraction, library preparation, and sequencing

RNA high-throughput sequencing, including lncRNA, miRNA, and mRNA of kidney tissues was conducted on BGI Technology Service Co. Ltd (Shenzhen, China). In brief, total RNA was extracted from kidney tissues using a TRIzol reagent (Invitrogen, CA, USA) according to the manufacturer's instructions. RNA concentration and integrity were assessed using the Qubit® 3.0 Fluorometer (Thermo Fisher, MA, USA) and the Agilent 2100 Bioanalyzer (Agilent Technologies Inc., CA, USA), respectively. Then, the MGIEasy Small RNA Library Prep Kit (MGI, Shenzhen, China) was used to construct the miRNA library. In terms of lncRNA and mRNA, libraries were prepared using the BGI Optimal series two-module mRNA Library Construction Kit (MGI, Shenzhen, China) following the manufacturer's protocol. Subsequently, the qualified libraries of miRNA, lncRNA, and mRNA were sequenced on the Genetic Sequencer MGISEQ-2000 (MGI, Shenzhen, China), and raw reads were generated. SOAPnuke software (v1.5.2) was employed to filter out raw reads that contained sequencing adapter, low-quality, as well as unknown base ratio > 5 %, and high-quality clean reads were obtained for the following analysis.

2.4. Identification of differentially expressed mRNAs, miRNAs, and lncRNAs

Differential expression statistics were performed using DESeq2 (v1.4.5), a R package. DE lncRNAs, miRNAs, and mRNAs were screened by a threshold of $|\log2 \text{ (fold change)}| \geq 1$ and adjusted P value < 0.05, and were visualized by a volcano plot.

2.5. Identification of differentially expressed cuproptosis-related genes and prediction

In total, 2056 cuproptosis-related genes (CRGs) were acquired from previous literature [10,22–26]' which were merged with differentially expressed mRNAs in sequencing analysis to obtain differentially expressed cuproptosis-related genes (DE-CRGs) in DKD rats. Based on the DE-CRGs, RNAhybrid, Miranda, and TargetScan were used to predict miRNAs and lncRNAs. Whereafter, the intersection between the predicted miRNAs and lncRNAs and the sequenced DE-miRNAs and DE-lncRNAs was performed by Venn diagram to acquire DE-cuproptosis-related miRNAs and lncRNAs.

2.6. Construction of cuproptosis-related lncRNA-miRNA-mRNA network

The relationship between cuproptosis-related lncRNA-miRNA and miRNA-mRNA was carried out using Spearman correlations analysis. LncRNA-miRNA pairs and miRNA-mRNA pairs with $|\text{correlation coefficient}| \geq 0.80$ and p-value <0.05 were screened out for cuproptosis-related ceRNA network construction. In addition, a hub cuproptosis-related ceRNA network was established based on the inversely regulatory relationship pairs and the threshold value of degree that was calculated using CytoNCA, a plugin of Cytoscape 3.8.0.

2.7. GO and KEGG enrichment analysis of DE-CRGs in the ceRNA network

GO and KEGG enrichment analysis of DE-CRGs were conducted using R "Phyper function" based on the Hypergeometric test and ClueGO, a plugin of Cytoscape 3.8.0. GO terms and KEGG pathways with a threshold of p-value <0.05 were regarded as significant enrichment.

2.8. Screening and analysis of hub DE-CRGs

Protein-protein interaction (PPI) network of DE-CRGs was established using STRING (https://string-db.org) with default values to reveal the interaction between genes and was visualized by Cytoscape (v 3.8.0). CytoNCA and CytoHubba, plugins of Cytoscape 3.8.0, were employed to calculate the value of each node gene based on 13 algorithms, Betweenness (BC), Closeness (CC), Degree (DC), Eigenvector (EC), Local Average Connectivity (LAC), Network (NC), Maximal Clique Centrality (MCC), Density of Maximum Neighborhood Component (DMNC), Maximum Neighborhood Component (MNC), Edge Percolated Component (EPC), BottleNeck, EcCentricity, along with Radiality. The top genes were screened based on the above algorithms by the R package "UpSet", which differential expression between the CON and MOD groups were exhibited by the box plot and heatmap. According to Spearman's statistical method, the R package "corrplot" was used to analyze the correlation of hub DE-CRGs.

2.9. Evaluation of immune cell infiltration

CIBERSORT algorithm, a method for estimating different immune cell types, was used to calculate the relative proportion of 22 infiltrating immune cell types in each sample. Accurate immune cell fractions were identified using a threshold of p-value <0.05 as screening criteria. The relationship between hub DE-CRGs and immune cells associated with DKD was performed using Spearman's statistical method, with a threshold of $|\text{correlation coefficient}| \geq 0.80$ and p-value <0.05 indicating a significant association.

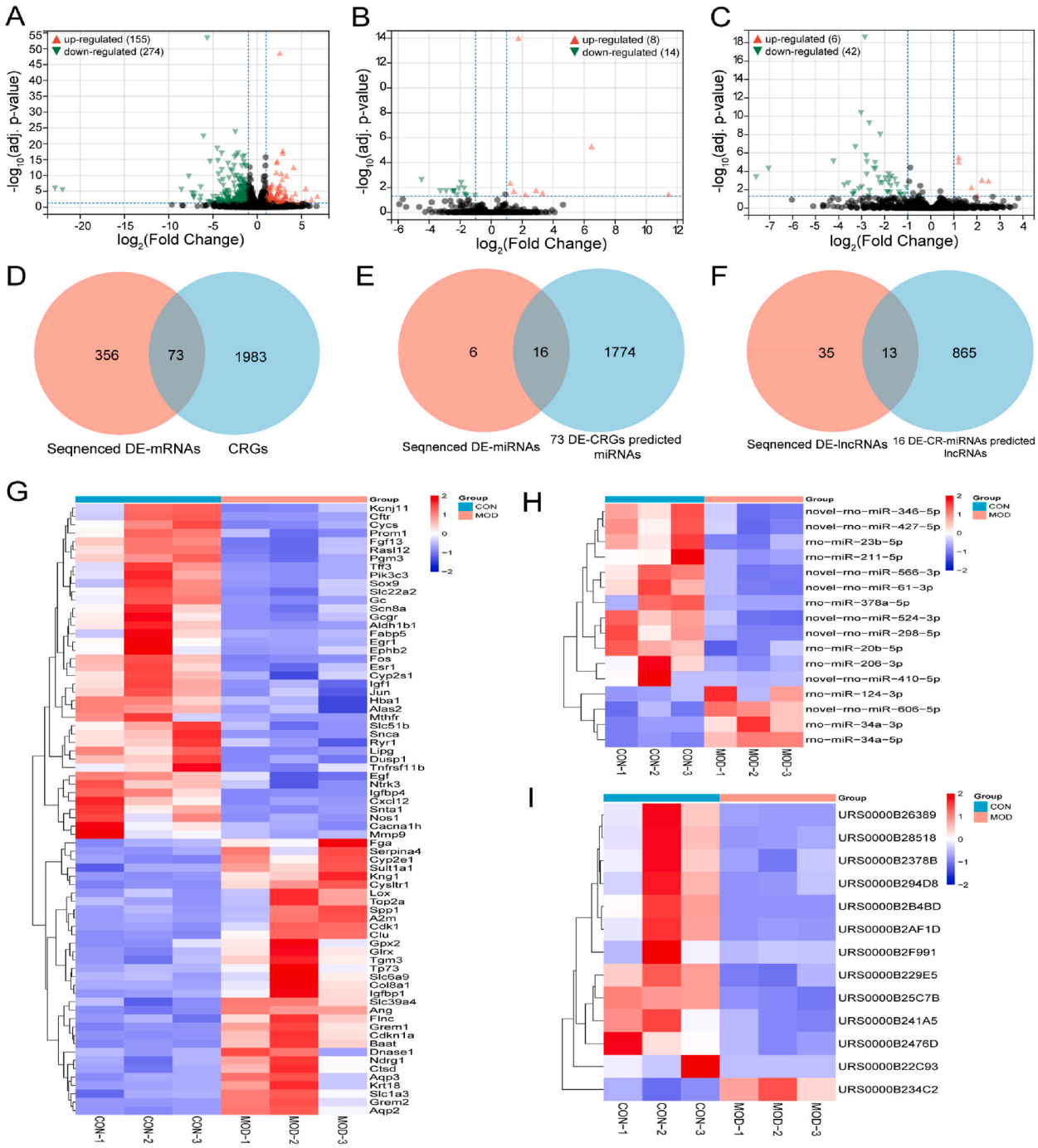

Fig. 3. The mRNAs, miRNAs, and lncRNAs between CON and MOD groups. (A) Volcano plot of differentially expressed mRNAs. (B) Volcano plot of differentially expressed miRNAs. (C) Volcano plot of differentially expressed lncRNAs. (D) Venn diagram of differentially expressed mRNAs and cuproptosis-related genes. (E) Venn diagram of differentially expressed miRNAs and predicted miRNAs. (F) Venn diagram of differentially expressed lncRNAs and predicted lncRNAs. (G) The heatmap of 73 differentially expressed cuproptosis-related genes. (H) The heatmap of 16 differentially expressed cuproptosis-related miRNAs. (I) The heatmap of 13 differentially expressed cuproptosis-related lncRNAs. DE, differentially expressed; CRGs, cuproptosis-related genes.

3. Results

3.1. Histological analysis of DKD rats

To evaluate whether the DKD model has been successfully constructed, Periodic acid-Schiff (PAS) staining was used to observe the histopathological features of DKD rats. It can be seen that the size of the kidney was markedly enlarged in the MOD group compared to the CON group (Fig. 2B). The results of the PAS staining as shown in Fig. 2C, the kidney tissue of rats in the CON group showed a clear and thin glomerular capillary loop, a normal number of mesangial cells, and a clear basement membrane. In contrast, rats in the MOD group exhibited severe pathological damages with obvious mesangial cell proliferation, hypertrophy of the glomerular capillary loop, and thickening of the basement membrane (Fig. 2C). These results indicated that the DKD model had been successfully constructed, and there was a pronounced renal injury in DKD rats.

3.2. Expression profiles of mRNA, miRNA, and lncRNA

To explore the differential gene expression in DKD rats, the transcriptome profiles of mRNA, miRNA, and lncRNA were investigated from three DKD rats and three control samples. In total, there were 18823 mRNAs, 1336 miRNAs, and 2741 lncRNAs.

3.2.1. mRNA profiles and cuproptosis-related DEGs identification

The volcano plot of mRNAs is shown in Fig. 3A, 429 mRNAs were significantly different between CON and MOD groups, of which 155 and 274 mRNAs were up-regulated and down-regulated, respectively (Table S1). In addition, differentially expressed mRNAs were merged with cuproptosis-related genes, and a total of 73 DE-CRGs were obtained for further analysis (Fig. 3D and G).

3.2.2. miRNA profiles and target miRNA prediction

A comparison of expression profile data from rats in CON and MOD groups identified 22 significantly different miRNAs with eight up-regulated and 14 down-regulated (Fig. 3B). Furthermore, 1790 predicted miRNAs were obtained based on the above 73 DE-CRGs using MiRanda, TargetSCan 8.0, and RNAhybrid. Among them, 16 DE-CR-miRNAs co-existed in the sequenced miRNAs and predicted miRNAs (Fig. 3E and H).

3.2.3. LncRNA profiles and target lncRNA prediction

With the screening criteria of lncRNA mentioned above, 48 significantly different lncRNAs were identified in CON and MOD groups, including six up-regulated and 42 down-regulated lncRNAs (Fig. 3C). In all, 878 predicted-lncRNAs were acquired based on the above 16 DE-CR miRNAs via MiRanda, TargetSCan 8.0, and RNAhybrid. Subsequently, 878 predicted-lncRNAs were integrated with 48 sequenced lcnRNAs, and ultimately 13 overlapping lncRNAs were acquired for further analysis (Fig. 3F and I).

3.3. Construction of cuproptosis-related lncRNA-miRNA-mRNA regulatory network

To elucidate how lncRNAs and miRNAs exhibited the regulatory roles in DKD rats via targeting downstream cuproptosis-related genes, the interaction among significantly different lncRNAs, miRNAs, and mRNAs was constructed. Firstly, the correlation analysis between 13 DE-lncRNAs and 16 DE-miRNAs and 16 DE-miRNAs and 73 DE-mRNAs was conducted, and they were depicted in Figure S1 and Figure S2 using heatmaps, respectively. Subsequently, we screened out 59 lncRNA-miRNA pairs and 450 miRNA-mRNA pairs based on a cut-off with correlation coefficient value ≥ 0.80 or ≤ -0.8 and $P < 0.05$, and a cuproptosis-related ceRNA network that included 12 lncRNAs, 16 miRNAs, and 71 mRNAs was established (Fig. 4A). To deeply explore the pivotal roles of the ceRNA network, the top 40 scored node genes of the cuproptosis-related ceRNA network were obtained based on the above nine algorithms (Table S2) and were employed to screen the hub ceRNA network using the R package “UpSet”, and 25 node genes were obtained (Fig. 4B), which consisted of one lncRNA, six miRNAs, and 18 mRNAs (Fig. 4C). Of note, the hub ceRNA network showed that the USR0000B2476D lncRNA was negatively regulatory with rno-miR-34a-3p, and rno-miR-34a-3p was negatively regulatory with eight genes, namely, Mmp9, Pik3c3, Prom1, Snta1, Slc51b, Ntrk3, Snca, and Egf (Fig. 4D), indicating that the core ceRNA network that consisted of USR0000B2476D, miR-34a-3p, and eight genes may involve in the progression of DKD.

3.4. GO and KEGG analysis of the cuproptosis-related mRNAs in the ceRNA network

To further identify the biological processes of 73 cuproptosis-related mRNAs in DKD rats, GO and KEGG pathway analyses were conducted. According to the GO annotation analysis of cuproptosis-related mRNAs, a total of 977 GO items were obtained ($P < 0.05$), of which 719 items, 84 items, and 174 items were in BP, CC, and MF, respectively (Table S3). As can be seen from Fig. 5A, GO biological processes were mainly involved in response to xenobiotic stimulus (GO:0009410), response to drug (GO:0042493), aging (GO:0007568), etc., in BP, extracellular space (GO:0005615), extracellular region (GO:0005576), protein-containing complex (GO:0032991), etc., in CC, protein binding (GO:0005515), enzyme binding (GO:0019899), growth factor binding (GO:0019838), etc., in MF. Concerning the KEGG pathways analysis, 22 pathways were significantly enriched ($P < 0.05$) after eliminating pathways that belong to human diseases, such as Apelin signaling pathway, Apoptosis, Arginine and proline metabolism, MAPK signaling pathway, IL-17 signaling pathway, and TNF signaling pathway (Fig. 5B and Table S4).

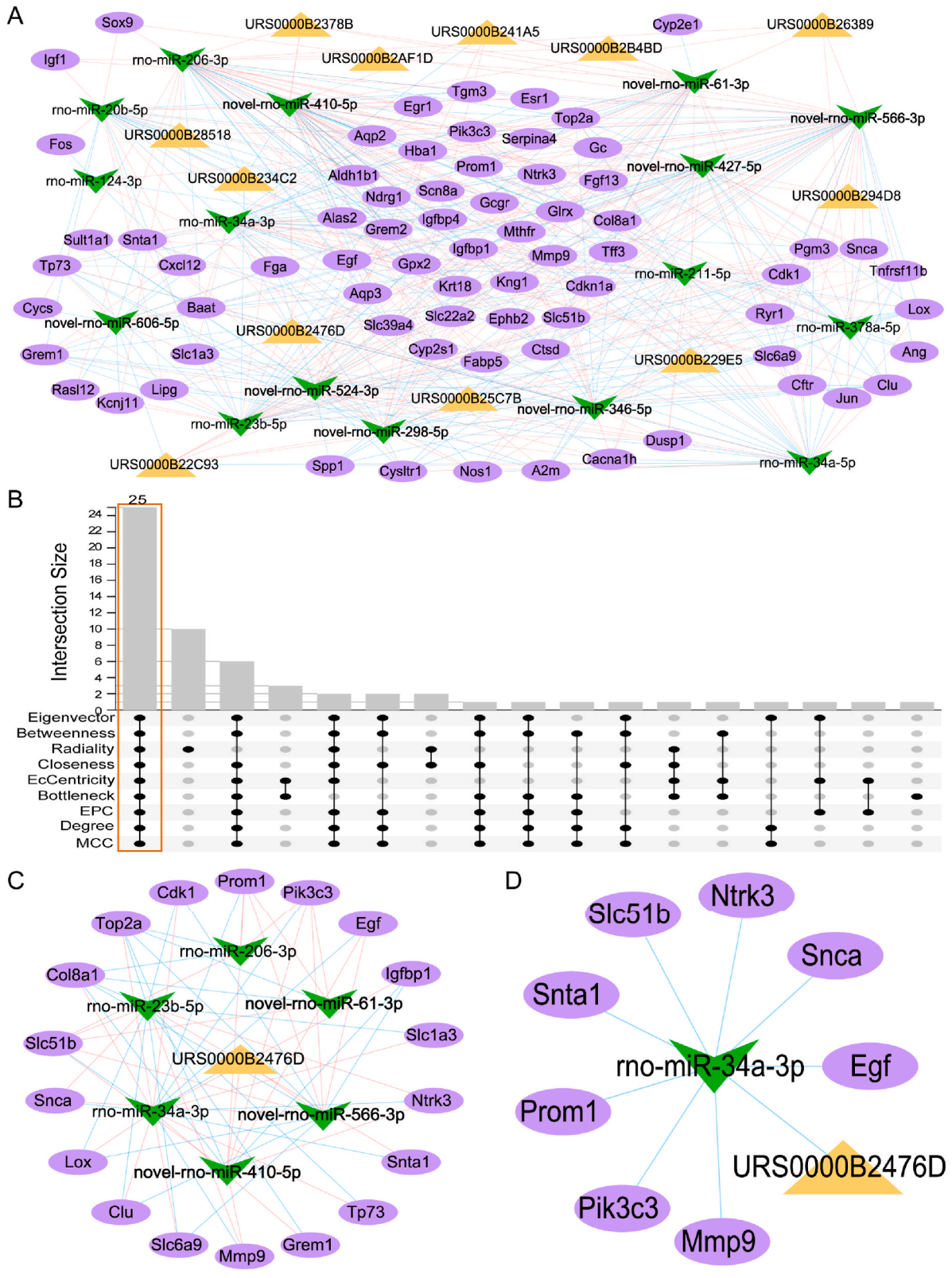

(caption on next page)

Fig. 4. Construction of cuproptosis-related lncRNA-miRNA-mRNA regulatory network. (A) The lncRNA–miRNA–mRNA regulatory network. (B) The upset plot of screening the hub ceRNA network. (C) The hub ceRNA network. (D) The core ceRNA network. The purple ellipses, green arrows, and orange triangles represent mRNAs, miRNAs, and lncRNAs, respectively. The color of the lines represents the relationship among mRNAs, miRNAs, and lncRNAs. The red lines represent positive correlation, while blue lines represent negative correlation.

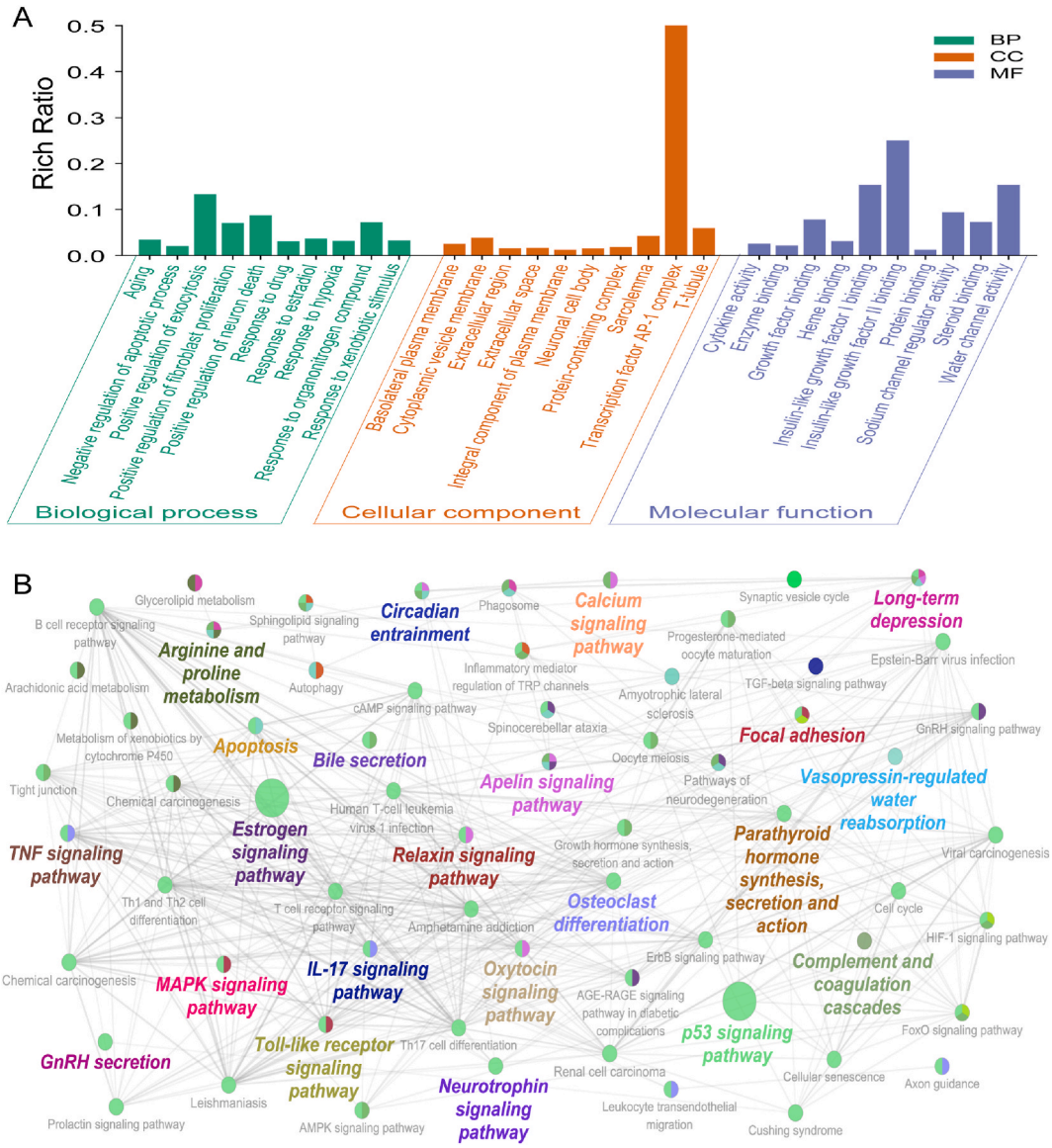

Fig. 5. GO and KEGG analysis of DE-CRGs in the ceRNA network. (A) Top ten GO enrichment annotations of biological process, cellular component, and molecular function. (B) KEGG pathways with bold font in color were significantly enriched ($P < 0.05$).

3.5. Identification and integration analyses of hub DE-CRGs

To obtain the hub DE-CRGs for subsequent analysis, a PPI network was constructed based on the above 73 DE-CRGs, and two Cytoscape plugins CytoNCA and CytoHubba were utilized to identify hub DE-CRGs according to the score of each node genes. Eventually, the top 30 scored node genes of 73 DE-CRGs were used to identify hub DE-CRGs using the R package "UpSet", and 18 hub DE-CRGs were obtained (Fig. 6A). The differential expression of 18 hub DE-CRGs between normal rats and DKD rats is presented in the heatmap (Fig. 6B) and boxplot (Fig. 6C). Of these, six hub DE-CRGs (Cdk1, Cdkn1a, Cyp2e1, Gpx2, Krt18, Spp1) were significantly up-regulated in DKD rats, whereas other 12 hub DE-CRGs (Cycs, Egf, Egr1, Esr1, Fos, Igf1, Jun, Mmp9, Nos1, Prom1, Snca, Sox9) were markedly down-regulated in DKD rats. In terms of the correlation analysis of hub DE-CRGs, there were multiple pairs with strong

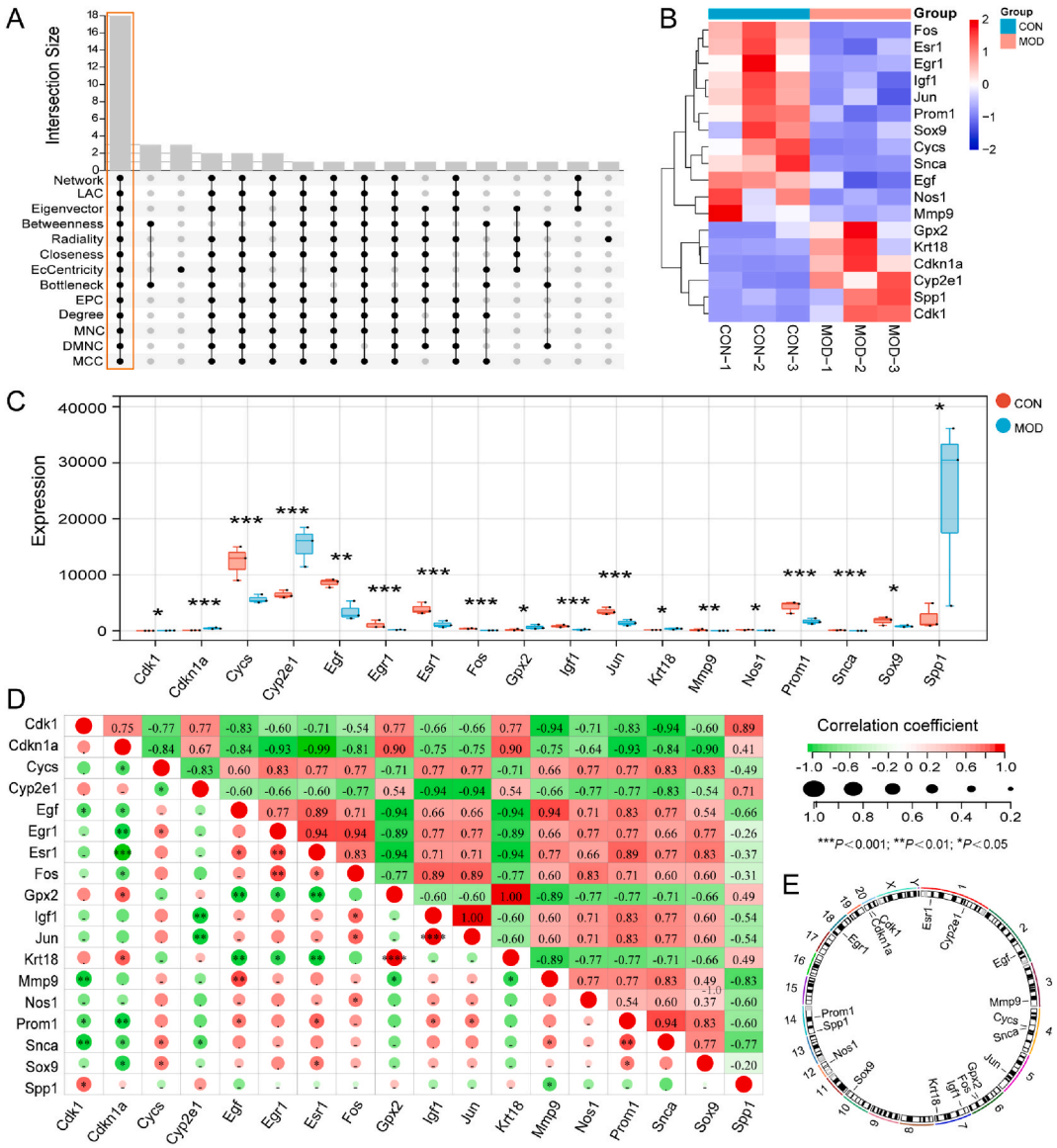

Fig. 6. Identification and integration analysis of hub DE-CRGs in DKD. (A) The upset plot of screening the hub DE-CRGs. (B) The heatmap of the differential expression of hub DE-CRGs between normal and DKD rats. (C) The boxplot of the differential expression of hub DE-CRGs between normal and DKD rats. (D) Correlation analysis of hub DE-CRGs. Red and Green colors represent positive and negative correlations, respectively. (E) The location of hub DE-CRGs on chromosomes. ***$P < 0.001$, **$P < 0.01$, *$P < 0.05$.

positive or negative correlations with coefficient absolute value ≥ 0.8 and p-value < 0.05, such as Cdk1 and Spp1 (0.89), Cdkn1a and Sox9 (−0.90), Snca and Prom1 (0.94), Mmp9 and Cdk1 (−0.93), as well as Cdkn1a and Esr1 (−0.99) (Fig. 6D), indicating that these hub DE-CRGs pairs may exert synergistic or antagonistic effects in the onset and progression of DKD. From the circle plot of chromosomal positions, we can see that hub DE-CRGs were located on chromosomes 1, 2, 3, 4, 5, 6, 7, 10, 12, 14, 18, and 20 (Fig. 6E).

3.6. *Immune cell infiltration analysis of hub DE-CRGs*

To explore whether there are immune system differences between normal and DKD rats, the immune infiltration analysis of hub DE-CRGs was performed using the CIBERSORT algorithm. The proportions of 22 immune cell infiltration of hub DE-CRGs are exhibited in Fig. 7A, which were mainly focused on native B cells, memory-activated $CD4^+$ T cells, as well as Monocytes. The differential analysis of immune cells showed that resting dendritic cells, resting NK cells, and regulatory T cells significantly differed between normal and DKD rats, of which resting dendritic cells and resting NK cells were up-regulated and regulatory T cells were down-regulated in DKD rats (Fig. 7B). We subsequently carried out the correlation analysis of 18 hub DE-CRGs and immune cells, and found that hub DE-CRGs

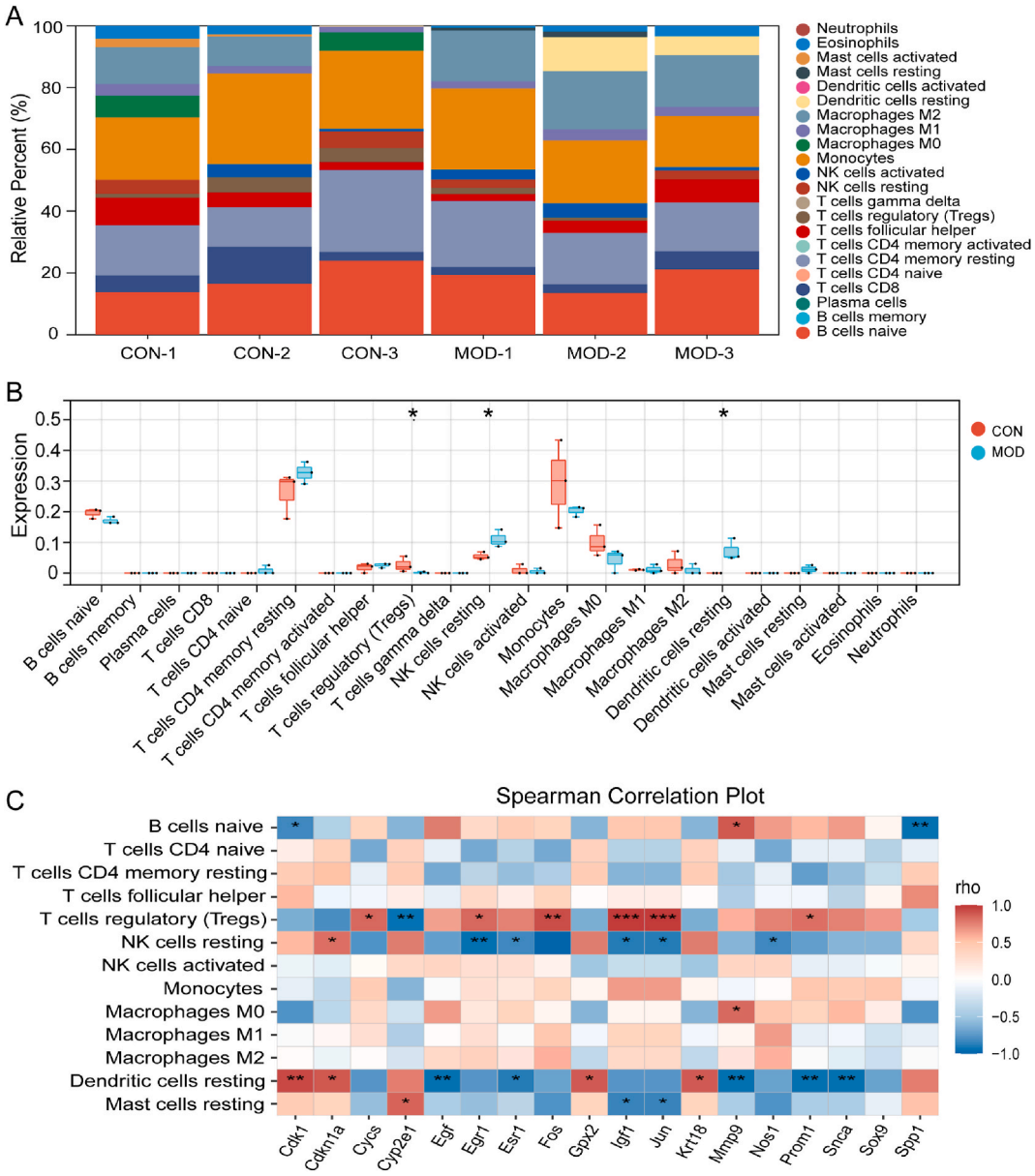

Fig. 7. Immune cell infiltration analysis of hub DE-CRGs in DKD. (A) The relative abundances of 22 infiltrated immune cells between normal and DKD rats. (B) Boxplots showed the differences in immune infiltrating between normal and DKD rats. (C) Correlation analysis between 18 hub DE-CRGs and infiltrated immune cells. ***$P < 0.001$, **$P < 0.01$, *$P < 0.05$.

showed significant correlations with native B cells, regulatory T cells, resting NK cells, M0 macrophages, resting dendritic cells, along with resting mast cells (Fig. 7C). Regulatory T cells were dramatically positively linked to Cycs, Egr1, Fos, Igf1, Jun, as well Prom1. Resting NK cells were significantly inversely associated with Egr1, Esr1, Igf1, Jun, and Nos1, while had a positive correlation with Cdkn1a. Resting dendritic cells showed markedly negatively linked to Egf, Esr1, Mmp9, Prom1, and Snca, and positively linked to Cdk1, Cdkn1a, Gpx2, and Krt18. These findings suggested that hub DE-CRGs may play critical roles in immune infiltration in DKD.

4. Discussion

DKD, a currently main cause of renal replacement therapy, places a huge physical and financial burden on patients and has become a global severe health challenge [27]. As the concrete mechanisms of DKD are not yet clear, conventional therapeutic management provides only finite effectiveness benefits and there is no foolproof solution to prevent end-stage renal disease. Cuproptosis, a novel form of mitochondrial cell death, has recently been discovered. And cuproptosis-related ceRNA networks contribute to disease

progression. To our knowledge, this is the first study to construct a regulatory circRNA-miRNA-mRNA network and immune infiltration in DKD based on cuprotosis. We found pronounced renal histopathological damage in DKD rats. There were significantly different 429 mRNAs, 22 miRNAs, and 48 lncRNAs in CON and MOD rats, and a total of 73 DE-CRGs, 16 DE-CR-miRNAs, and 13 DE-CR-lncRNAs were identified, respectively. A cuproptosis-related ceRNA network that included 12 lncRNAs, 16 miRNAs, and 71 mRNAs was established. In addition, the core ceRNA network consisted of USR0000B2476D, miR-34a-5p, and eight genes. GO and KEGG pathway analysis of 73 DE-CRGs showed that 977 GO items and 22 pathways were significantly enriched. What's more, 18 hub DE-CRGs were obtained, which showed significant correlations with native B cells, regulatory T cells, resting NK cells, M0 macrophages, resting dendritic cells, and resting mast cells. These findings may provide a novel understanding of the pathogenesis of DKD.

The ceRNA is a network that reveals the interaction of different RNAs and keeps a relatively balanced. When the balance is disturbed, it will cause diseases. In our study, a cuproptosis-related ceRNA network was constructed, which consisted of USR0000B2476D, miR-34a-3p, and eight mRNAs. Among them, mRNAs mainly included Mmp9, Pik3c3, Prom1, Snta1, Slc51b, Ntrk3, Snca, and Egf. LncRNAs can act as ceRNAs to protect mRNAs from miRNA inhibition [28]. USR0000B2476D, a lncRNA, has not been reported in previous studies. In the present study, USR0000B2476D was downregulated and was negatively regulatory with rno-miR-34a-3p in DKD rats, indicating the down expression of USR0000B2476D may lead to DKD pathological process and protect mRNAs via inhibiting rno-miR-34a-3p in DKD. MiR-34a is a class of small single-stranded noncoding RNA, which is involved in the development and progression of DKD by forming a complex network with targeted genes such as Sirt1/HIF-1α [29]. We found that the level of miR-34a was upregulated in DKD rats ， which is consistent with previous studies [30,31]. In addition, miR-34a may exhibit its pathogenic roles in DKD by regulating the function of target genes, including Mmp9, Pik3c3, Prom1, Snta1, Slc51b, Ntrk3, Snca, and Egf.

Matrix metalloproteinase-9 (Mmp9) is one of the members of the matrix metalloproteinase family, which plays a pivotal role in the synthesis and degradation of the extracellular matrix (ECM) and is involved in the development of renal fibrosis [32]. Dysfunctionality of Mmp9 is closely associated with the ECM regulation in DKD, which makes Mmp9 a a potential target for therapeutic intervention in DKD. It has been demonstrated that the elevated MMP-9 induced excessive renal ECM accumulation, of which the increased MMP-9 was shown incapable of degrading nonenzymatically glycated collagen IV that contributed to thickening of the glomerular basement membrane, a hallmark of DKD [33]. Other studies also proved that the expression of Mmp9 significantly increased in high glucose-induced podocytes [34], DKD rats [35], and DKD patients [36]. In contrast, previous studies showed a marked downregulation of MMP-9 in DKD rats [37,38]. Our current study showed that MMP-9 was significantly decreased in DKD rats. Therefore, the regulatory mechanism of Mmp9 on DKD needs to be explored in the future.

PIK3C3, also known as Vacuolar protein sorting 34 (VPS34), is a member of the family of phosphoinositide 3-kinases—lipid kinases that play a crucial role in autophagy regulation and has received much attention [39]. Autophagy is essential to the maintenance of cellular homeostasis in renal cells, and disorder in autophagy is considered the main reason for the accumulation of damaged proteins and organelles in diabetic renal cells [40]. Abnormal autophagy mediated by the dysregulation of PIK3C3 is closely related to the pathological progression of various diseases, including DKD. Zhang et al. found that the level of autophagy-related protein VPS34 was lower in the renal tissues of db/db mice than in the control mice [41]. Consistent with the finding of Zhang et al. the expression of PIK3C3 was also decreased in DKD rats in the present study.

Prominin-1 (Prom1) is an integral membrane protein that is related to the plasma membrane. It has been reported that loss of Prom1 impaired autophagy and promoted epithelial-mesenchymal transition in mouse retinal pigment epithelial cells [42]. However, the role of Prom1 in DKD has not been reported in previous studies. Alpha-1-syntrophin (SNTA1), a peripheral cytoplasmic membrane protein, is associated with the dystrophin-glycoprotein complex in muscle cells and other mammalian tissues [43].

Solute carrier 51 β (SLC51B) is a member of the human solute carrier family. Hepatocyte nuclear factor 1 A (HNF1A) is predominantly expressed in the kidneys. It has been proved that loss of HNF1A resulted in reduced SLC51B expression, which may decrease renal protection [44]. In the present study, the expression of SLC51B was markedly decreased; thus, we hypothesized that HNF1A may impaired in DKD rats, which needs to be confirmed in the future. Alpha-synuclein (SNCA), a presynaptic neuronal protein, has been reported to play an important role in the pathogenesis of Parkinson's disease. It has also been found to affect the mitochondrial features recently, namely, SNCA interacts with complex I, impairs its function, promotes the production of reactive oxygen species, and causes direct mitochondrial toxicity [45]. Mitochondrial dysfunction has been identified as a key event in the progression of DKD [46]. Therefore, restoring mitochondrial function by targeting SNCA may be a potential therapeutic strategy in preventing DKD progression. Epidermal growth factor (EGF) is a factor produced mainly in distal renal tubules, which has been considered a marker of renal injury [47]. However, how these genes regulate the cuproptosis in DKD needs to be confirmed by further in vivo and in vitro experiments.

Recently, immune-mediated inflammation has been regarded as a primary pathogenic mechanism in DKD [7]. Effector cells of adaptive immune responses, such as T-helper 1 cell (Th1), Th2, Th17, and regulatory T cells (Treg), are increased in patients with DKD, and the imbalance of Th 1/Th 2 and Th17/Treg has been proven to affect the development and progression of DKD [48]. Combining the immune infiltrating difference analysis results of hub DE-CRGs, we found that the proportions of 22 immune cell infiltration of hub DE-CRGs in DKD rats were mainly focused on native B cells, memory-activated $CD4^+$ T cells, along with Monocyte. In addition, in DKD rats, the infiltration of Treg decreased but that of resting dendritic cells and resting NK cells increased. Treg cells, as a potent immunosuppressive, exert central roles in the maintenance of immune homeostasis and tolerance via producing anti-inflammatory cytokines, such as IL-10, and transforming growth factor-β [49]. Previous studies showed that the proportion of Th17 cells increased while Treg cells decreased and the imbalance of Th17/Treg in DKD patients and DKD rats [48,50]. In line with these reports, we found that the proportion of Treg was significantly decreased. It has been demonstrated that CD4(+) T cell activation by resting dendritic cells induced helper function and promoted the expansion and differentiation of cognate CD8(+) T cells [51]. In terms of

resting NK cells, M1 Macrophages activated it via the engagement of IL-1β, IFN-β, and IL-15 Pathways [52]. In the present study, we found a higher proportion of resting dendritic cells and resting NK cells in DKD rats than in controls. However, the roles of resting dendritic cells and resting NK cells in DKD remain unclear. Furthermore, we also analyzed the correlation between cuproptosis-related genes and immune cells. These findings showed that regulatory T cells were positively associated with Cycs, Egr1, Fos, Igf1, Jun, and Prom1, resting NK cells were inversely associated with Egr1, Esr1, Igf1, Jun, and Nos1, and resting dendritic cells had markedly linked to Egf, Esr1, Mmp9, Prom1, and Snca, etc., which may provide information for the correlation between DKD immunity and the cuproptosis mechanism.

Further KEGG analysis of CR-DEGs in DKD rats' samples illustrated that CR-DEGs were mainly enriched in the MAPK signaling pathway, IL-17 signaling pathway, TNF signaling pathway, etc. As a well-known canonical pro-inflammatory pathway, the MAPK pathway has been proven to be activated in DKD mice [53]. Consistent with previous findings, we found that the MAPK pathway was activated in DKD rats. IL-17 acts as a critical regulator of innate immunity and has been implicated in several inflammatory diseases, but its role in DKD has been conflicting. Ma et al. reported that diabetic IL-17A deletion mice displayed a reduction in albuminuria and an improvement in glomerular damage and fibrosis, indicating that IL-17A signaling may accelerate the pathogenesis of DKD [54]. In contrast, Mohamed et al. found that IL-17A levels were reduced in patients with DKD and diabetic mice deficient in IL-17A developed more severe kidney damage, while administration of low-dose IL-17 was sufficient to suppress DKD [55]. Therefore, the specific roles of IL-17 in DKD still need further study. TNF, a proinflammatory cytokine, can aggravate the renal inflammatory response by activating the NF-κB signaling pathway and MAPK cascade, thereby leading to the progression of DKD [56]. Therefore, these CR-DEGs may contribute to the progression of DKD by mediating these pathways that are closely associated with immunity and inflammation.

5. Conclusions

In this study, we explored a cuproptosis-related lncRNA-miRNA-mRNA network and immune infiltration in DKD that originated from RNA high-throughput sequencing for the first time. Generally, the cuproptosis-related core ceRNA network consisted of USR0000B2476D, miR-34a-3p, and eight genes (Mmp9, Pik3c3, Prom1, Snta1, Slc51b, Ntrk3, Snca, and Egf), which may involve in the pathogenesis of DKD. In addition, eighteen hub DE-CRGs (Cdk1, Cdkn1a, Cyp2e1, Gpx2, Krt18, Spp1, Cycs, Egf, Egr1, Esr1, Fos, Igf1, Jun, Mmp9, Nos1, Prom1, Snca, and Sox9) play important roles in the pathogenesis of immune infiltration in DKD, and resting dendritic cells, resting NK cells, and regulatory T cells were disordered in DKD. In all, these findings provide new insights into the non-coding RNAs and cuproptosis mechanisms of DKD, although experiments remain indispensable for validation in further research.

Data availability statement

The original contributions presented in the study are included in the article/supplementary materials. All data was reproducible in this experiment.

Ethics statement

The experimental procedures of our study were reviewed and approved by the Institutional Welfare and Ethics Committee of Guangxi University of Chinese Medicine (approval No. DW20210927-163).

Funding

This research was supported by grants from NATCM's Project of High-level Construction of Key TCM Disciplines (zyyzdxk-2023166); Guangxi Natural Science Foundation Project (2023GXNSFBA026209); Guangxi University of Chinese Medicine Introduced Doctoral Research Start-up Fund Project (2023BS038).

CRediT authorship contribution statement

Fang Lan: Writing – original draft, Visualization, Investigation, Formal analysis, Conceptualization. **Jie Zhao:** Writing – original draft, Validation, Investigation. **Dan Liang:** Software, Methodology, Data curation. **Chao Mo:** Writing – review & editing, Project administration, Conceptualization. **Wei Shi:** Writing – review & editing, Project administration, Funding acquisition.

Declaration of competing interest

The authors declare that they have no known competing financial interests or personal relationships that could have appeared to influence the work reported in this paper.

Appendix B. Supplementary data

Supplementary data to this article can be found online at https://doi.org/10.1016/j.heliyon.2024.e35700.

References

[1] International Diabetes Federation, International DiabetesFederation diabetes Atlas , 10th [2024-03-16], https://www.diabetesatlas.org, 2021-11-08.
[2] R.M. Zhang, F. Persson, J.B. McGill, P. Rossing, Clinical implications and guidelines for CKD in type 2 diabetes, Nephrol. Dial. Transplant. 38 (2023) 542–550.
[3] S. Gupta, M. Dominguez, L. Golestaneh, Diabetic kidney disease: an update, Med Clin North Am 107 (2023) 689–705.
[4] B.M. Scirica, O. Mosenzon, D.L. Bhatt, J.A. Udell, P.G. Steg, D.K. McGuire, K. Im, E. Kanevsky, C. Stahre, M. Sjöstrand, I. Raz, E. Braunwald, Cardiovascular outcomes according to urinary albumin and kidney disease in patients with type 2 diabetes at high cardiovascular risk: observations from the SAVOR-TIMI 53 trial, JAMA Cardiol 3 (2018) 155–163.
[5] A. Levin, M. Tonelli, J. Bonventre, J. Coresh, J.A. Donner, A.B. Fogo, C.S. Fox, R.T. Gansevoort, H.J.L. Heerspink, M. Jardine, B. Kasiske, A. Köttgen, M. Kretzler, A.S. Levey, V.A. Luyckx, R. Mehta, O. Moe, G. Obrador, N. Pannu, C.R. Parikh, V. Perkovic, C. Pollock, P. Stenvinkel, K.R. Tuttle, D.C. Wheeler, K.U. Eckardt, Global kidney health 2017 and beyond: a roadmap for closing gaps in care, research, and policy, Lancet 390 (2017) 1888–1917.
[6] J.L. Harding, M.E. Pavkov, D.J. Magliano, J.E. Shaw, E.W. Gregg, Global trends in diabetes complications: a review of current evidence, Diabetologia 62 (2019) 3–16.
[7] R.A. DeFronzo, W.B. Reeves, A.S. Awad, Pathophysiology of diabetic kidney disease: impact of SGLT2 inhibitors, Nat. Rev. Nephrol. 17 (2021) 319–334.
[8] G. Gervasini, Recent advances and remaining challenges in the management of diabetic kidney disease, J. Clin. Med. 12 (2023) 2759.
[9] P.A. Cobine, S.A. Moore, S.C. Leary, Getting out what you put in: copper in mitochondria and its impacts on human disease, Biochim. Biophys. Acta Mol. Cell Res. 1868 (2021) 118867.
[10] P. Tsvetkov, S. Coy, B. Petrova, M. Dreishpoon, A. Verma, M. Abdusamad, J. Rossen, L. Joesch-Cohen, R. Humeidi, R.D. Spangler, J.K. Eaton, E. Frenkel, M. Kocak, S.M. Corsello, S. Lutsenko, N. Kanarek, S. Santagata, T.R. Golub, Copper induces cell death by targeting lipoylated TCA cycle proteins, Science. 375 (2022) 1254–1261.
[11] Y. Wang, L. Zhang, F. Zhou, Cuproptosis: a new form of programmed cell death, Cell. Mol. Immunol. 19 (2022) 867–868.
[12] C. Bian, Z. Zheng, J. Su, S. Chang, H. Yu, J. Bao, Y. Xin, X. Jiang, Copper homeostasis and cuproptosis in tumor pathogenesis and therapeutic strategies, Front. Pharmacol. 14 (2023) 1271613.
[13] L. Yang, P. Yang, G.Y.H. Lip, J. Ren, Copper homeostasis and cuproptosis in cardiovascular disease therapeutics, Trends Pharmacol. Sci. 44 (2023) 573–585.
[14] Q. Wang, J. Sun, T. Chen, S. Song, Y. Hou, L. Feng, C. Fan, M. Li, Ferroptosis, pyroptosis, and cuproptosis in Alzheimer's disease, ACS Chem. Neurosci. 14 (2023) 3564–3587.
[15] L. Wang, K. Xiao, Z. Dong, T. Meng, X. Cheng, Y. Xu, A novel copper-induced cell death-related lncRNA prognostic signature associated with immune infiltration and clinical value in gastric cancer, J. Cancer Res. Clin. Oncol. 149 (2023) 10543–10559.
[16] Z. Zhu, T. Guo, J. Weng, S. Li, C. Zhu, Q. Zhao, Y. Xu, Cuproptosis-related miRNAs signature and immune infiltration characteristics in colorectal cancer, Cancer Med. 12 (2023) 16661–16678.
[17] W. Lian, P. Yang, L. Li, D. Chen, C. Wang, A ceRNA network-mediated over-expression of cuproptosis-related gene SLC31A1 correlates with poor prognosis and positive immune infiltration in breast cancer, Front. Med. 10 (2023) 1194046.
[18] C. Mo, J. Zhao, J. Liang, Y. Chen, H. Wang, Y. Dai, G. Huang, Effects of Zhuang medicine compound Xiancao Granule on diabetic kidney disease: a multi-omics analysis, J. Ethnopharmacol. 321 (2024) 117517.
[19] K.M. Park, K.H. Hussein, H.S. Nam, H.M. Kim, B.M. Kang, D.G. Lee, H.J. Han, H.M. Woo, A novel mouse model of diabetes mellitus using unilateral nephrectomy, Lab Anim 50 (2016) 88–93.
[20] H. Kim, T. Dusabimana, S.R. Kim, J. Je, K. Jeong, M.C. Kang, K.M. Cho, H.J. Kim, S.W. Park, Supplementation of abelmoschus manihot ameliorates diabetic nephropathy and hepatic steatosis by activating autophagy in mice, Nutrients 10 (2018) 1703.
[21] W. Wei, X.M. Wu, Y.J. Li, Methodology of Pharmacological Experiment, fourth ed., People's Medical Publishing House, Beijing, 2010, p. 1238.
[22] L. Zheng, X. Yang, Q. Fan, B. Liu, W. Hu, Y. Cui, Transcriptomic profiling identifies differentially expressed genes and related pathways associated with wound healing and cuproptosis-related genes in Ganxi goats, Front. Vet. Sci. 10 (2023) 1149333.
[23] H. Lv, X. Liu, X. Zeng, Y. Liu, C. Zhang, Q. Zhang, J. Xu, Comprehensive analysis of cuproptosis-related genes in immune infiltration and prognosis in melanoma, Front. Pharmacol. 13 (2022) 930041.
[24] T. Huang, Y. Liu, J. Li, B. Shi, Z. Shan, Z. Shi, Z. Yang, Insights into prognosis and immune infiltration of cuproptosis-related genes in breast cancer, Front. Immunol. 13 (2022) 1054305.
[25] S. Liu, J. Ge, Y. Chu, S. Cai, J. Wu, A. Gong, J. Zhang, Identification of hub cuproptosis related genes and immune cell infiltration characteristics in periodontitis, Front. Immunol. 14 (2023) 1164667.
[26] Z. Wang, Y. Wang, J. Yan, Y. Wei, Y. Zhang, X. Wang, X. Leng, Analysis of cuproptosis-related genes in Ulcerative colitis and immunological characterization based on machine learning, Front. Med. 10 (2023) 1115500.
[27] Q. Hu, Y. Chen, X. Deng, Y. Li, X. Ma, J. Zeng, Y. Zhao, Diabetic nephropathy: focusing on pathological signals, clinical treatment, and dietary regulation, Biomed. Pharmacother. 159 (2023) 114252.
[28] Y. Tay, J. Rinn, P.P. Pandolfi, The multilayered complexity of ceRNA crosstalk and competition, Nature 505 (2014) 344–352.
[29] A. Li, R. Peng, Y. Sun, H. Liu, H. Peng, Z. Zhang, LincRNA 1700020I14Rik alleviates cell proliferation and fibrosis in diabetic nephropathy via miR-34a-5p/Sirt1/HIF-1α signaling, Cell Death Dis. 9 (2018) 461.
[30] J.B. Hao, X.T. Liu, J. Tang, X.Y. Chang, H.G. Jin, B. Zhu, L.R. Hao, L. Zhang, The effect of allograft inflammatory factor-1 on inflammation, oxidative stress, and autophagy via miR-34a/ATG4B pathway in diabetic kidney disease, Oxid. Med. Cell. Longev. 2022 (2022) 1668000.
[31] S. Xiao, Y. Yang, Y.T. Liu, J. Zhu, Liraglutide regulates the kidney and liver in diabetic nephropathy rats through the miR-34a/SIRT1 pathway, J. Diabetes Res. 2021 (2021) 8873956.
[32] Y. Wang, L. Jiao, C. Qiang, C. Chen, Z. Shen, F. Ding, L. Lv, T. Zhu, Y. Lu, X. Cui, The role of matrix metalloproteinase 9 in fibrosis diseases and its molecular mechanisms, Biomed. Pharmacother. 171 (2024) 116116.
[33] J.D. Mott, R.G. Khalifah, H. Nagase, C.F. Shield 3rd, J.K. Hudson, B.G. Hudson, Nonenzymatic glycation of type IV collagen and matrix metalloproteinase susceptibility, Kidney Int. 52 (1997) 1302–1312.
[34] L. Ye, J.H. Chen, S.L. Zhu, D.D. Xu, Y. Yang, M.P. Shi, Hsa_circ_0001162 inhibition alleviates high glucose-induced human podocytes injury by the miR-149-5p/MMP9 signaling pathway, Appl. Biochem. Biotechnol. 195 (2023) 7255–7276.
[35] C. Ural, A. Celik, S. Ozbal, E. Guneli, S. Arslan, B.U. Ergur, C. Cavdar, G. Akdoğan, Z. Cavdar, The renoprotective effects of taurine against diabetic nephropathy via the p38 MAPK and TGF-β/Smad2/3 signaling pathways, Amino Acids 55 (2023) 1665–1677.
[36] E. Baldimtsi, P.A. Whiss, J. Wahlberg, Systemic biomarkers of microvascular alterations in type 1 diabetes associated neuropathy and nephropathy - a prospective long-term follow-up study, J Diabetes Complications 37 (2023) 108635.
[37] G. Alomari, B. Al-Trad, S. Hamdan, A.A.A. Aljabali, M.S. Al Zoubi, K. Al-Batanyeh, J. Qar, G.J. Eaton, A.K. Alkaraki, W. Alshaer, S. Haifawi, K. Jemon, D. K. Chellappan, K. Dua, M.M. Tambuwala, Alleviation of diabetic nephropathy by zinc oxide nanoparticles in streptozotocin-induced type 1 diabetes in rats, IET Nanobiotechnol. 15 (2021) 473–483.
[38] Y.B. Tripathi, R. Shukla, N. Pandey, V. Pandey, M. Kumar, An extract of Pueraria tuberosa tubers attenuates diabetic nephropathy by upregulating matrix metalloproteinase-9 expression in the kidney of diabetic rats, J. Diabetes 9 (2017) 123–132.
[39] L. Chen, T. Gao, P. Zhou, W. Xia, H. Yao, S. Xu, J. Xu, Recent advances of vacuolar protein-sorting 34 inhibitors targeting autophagy, Bioorg. Chem. 143 (2024) 107039.
[40] Y.P. Han, L.J. Liu, J.L. Yan, M.Y. Chen, X.F. Meng, X.R. Zhou, L.B. Qian, Autophagy and its therapeutic potential in diabetic nephropathy, Front. Endocrinol. 14 (2023) 1139444.
[41] X. Zhang, L. Zhang, Y. Wen, M. Zhang, S. Liu, H. Xiao, Vitamin D ameliorates podocyte injury by enhancing autophagy activity in diabetic kidney disease, Kidney Blood Press. Res. 48 (2023) 314–325.

[42] S. Bhattacharya, J. Yin, W. Huo, E. Chaum, Loss of Prom1 impairs autophagy and promotes epithelial-mesenchymal transition in mouse retinal pigment epithelial cells, J. Cell. Physiol. 238 (2023) 2373–2389.
[43] H.F. Bhat, R.A. Baba, M.E. Adams, F.A. Khanday, Role of SNTA1 in Rac1 activation, modulation of ROS generation, and migratory potential of human breast cancer cells, Br. J. Cancer 110 (2014) 706–714.
[44] J.W. Chan, C.W.Y. Neo, S. Ghosh, H. Choi, S.C. Lim, E.S. Tai, A.K.K. Teo, HNF1A binds and regulates the expression of SLC51B to facilitate the uptake of estrone sulfate in human renal proximal tubule epithelial cells, Cell Death Dis. 14 (2023) 302.
[45] C.J. Choong, H. Mochizuki, Involvement of mitochondria in Parkinson's disease, Int. J. Mol. Sci. 24 (2023) 17027.
[46] K.H. Cleveland, R.G. Schnellmann, Pharmacological targeting of mitochondria in diabetic kidney disease, Pharmacol. Rev. 75 (2023) 250–262.
[47] N.H. Johnson, R.W. Keane, J.P. de Rivero Vaccari, Renal and inflammatory proteins as biomarkers of diabetic kidney disease and lupus nephritis, Oxid. Med. Cell. Longev. 2022 (2022) 5631099.
[48] C. Zhang, C. Xiao, P. Wang, W. Xu, A. Zhang, Q. Li, X. Xu, The alteration of Th1/Th2/Th17/Treg paradigm in patients with type 2 diabetes mellitus: relationship with diabetic nephropathy, Hum. Immunol. 75 (2014) 289–296.
[49] K. Eller, A. Kirsch, A.M. Wolf, S. Sopper, A. Tagwerker, U. Stanzl, D. Wolf, W. Patsch, A.R. Rosenkranz, P. Eller, Potential role of regulatory T cells in reversing obesity-linked insulin resistance and diabetic nephropathy, Diabetes 60 (2011) 2954–2962.
[50] J. Wang, H. Liu, G. Yue, Y. Deng, W. Cai, J. Xu, Human placenta-derived mesenchymal stem cells ameliorate diabetic kidney disease by modulating the T helper 17 cell/regulatory T-cell balance through the programmed death 1/programmed death-ligand 1 pathway, Diabetes Obes Metab 26 (2024) 32–45.
[51] R.J. Steptoe, J.M. Ritchie, N.S. Wilson, J.A. Villadangos, A.M. Lew, L.C. Harrison, Cognate CD4+ help elicited by resting dendritic cells does not impair the induction of peripheral tolerance in CD8+ T cells, J. Immunol. 178 (2007) 2094–2103.
[52] I. Mattiola, M. Pesant, P.F. Tentorio, M. Molgora, E. Marcenaro, E. Lugli, M. Locati, D. Mavilio, Priming of human resting NK cells by autologous M1 macrophages via the engagement of IL-1β, IFN-β, and IL-15 pathways, J. Immunol. 195 (2015) 2818–2828.
[53] L. Ma, F. Wu, Q. Shao, G. Chen, L. Xu, F. Lu, Baicalin alleviates oxidative stress and inflammation in diabetic nephropathy via Nrf2 and MAPK signaling pathway, Drug Des Devel Ther 15 (2021) 3207–3221.
[54] J. Ma, Y.J. Li, X. Chen, T. Kwan, S.J. Chadban, H. Wu, Interleukin 17A promotes diabetic kidney injury, Sci. Rep. 9 (2019) 2264.
[55] R. Mohamed, C. Jayakumar, F. Chen, D. Fulton, D. Stepp, R.T. Gansevoort, G. Ramesh, Low-dose IL-17 therapy prevents and reverses diabetic nephropathy, metabolic syndrome, and associated organ fibrosis, J. Am. Soc. Nephrol. 27 (2016) 745–765.
[56] J. Lv, Z. Wang, Y. Wang, W. Sun, J. Zhou, M. Wang, W.J. Liu, Y. Wang, Renoprotective effect of the shen-yan-fang-shuai formula by inhibiting TNF-α/NF-κB signaling pathway in diabetic rats, J. Diabetes Res. 2017 (2017) 4319057.